Catalysis Today 158 (2010) 56–62

Contents lists available at ScienceDirect

Catalysis Today

journal homepage: www.elsevier.com/locate/cattod

Supported gold catalysts for CO oxidation and preferential oxidation of CO in H_2 stream: Support effect

L.F. Liotta*, G. Di Carlo, G. Pantaleo, A.M. Venezia

Istituto per lo Studio di Materiali Nanostrutturati, CNR, Via Ugo La Malfa, 90146 Palermo Italy

ARTICLE INFO

Article history:
Available online 22 June 2010

Keywords:
Au catalysts
TiO_2
CeO_2
Co_3O_4
Al_2O_3
CO oxidation
PROX reaction

ABSTRACT

Au catalysts on different type of reducible supports (TiO_2, Co_3O_4–CeO_2 mixed oxide, CeO_2, Co_3O_4) and over a non-reducible oxide, Al_2O_3, were prepared by deposition–precipitation method with Na_2CO_3 solution at pH 7–8, depending on the PZC of the supports. The as-prepared catalysts were characterized by BET, XRD, TEM and XPS techniques. The catalytic activity was investigated in the CO oxidation and in the preferential CO oxidation in the presence of hydrogen (PROX). The results were discussed in terms of nature of gold species and role of the support in the reaction mechanism.

1. Introduction

The electrochemical oxidation of hydrogen in low-temperature proton exchange membrane fuel cells (PEMFCs) has attracted much interest as an energy source for electric vehicles and residential power generators. The production of hydrogen by steam reforming of methanol or by partial oxidation of liquid hydrocarbons followed by water gas shift reaction generates gas effluents containing 0.3–1% of CO in an excess of H_2 (40–75%) and 20–25% of CO_2 [1,2]. Since the CO molecule present in the stream is detrimental for the metal electrodes anode used in fuel cells, especially Pt, it is important to reduce its level below 10 ppm [3]. The preferential oxidation (PROX) of CO is a possible way for removing trace amounts of CO from H_2 [4]. In a H_2-rich atmosphere, H_2 competes with CO to react with O_2, leading to decreased hydrogen generation. Therefore, to effectively remove CO from a H_2-rich atmosphere, a high amount of CO conversion with high selectivity, at the operating temperature of the fuel cells (80–100 °C), is required. Although there are still a lot of papers on PROX reaction over supported Pt and Pd catalysts [5,6], recently, it has been found that Au catalysts are effective candidates for PROX and potentially capable of being effectively employed in fuel cells [7]. Well-dispersed Au nanoparticles on reducible metal oxides have been found as active and selective catalysts for PROX at low temperature [8–10]. Moreover, it has been confirmed that the rate of CO oxidation over supported gold catalysts exceeds that of H_2 oxidation [11,12].

However, several factors such as Au particle size [13,14], oxidation state [15–17], nature of the support and length of the perimeter interface between gold particles and the support [18–20] affect the catalytic performance of gold catalysts toward CO oxidation at low-temperature. Most of the properties which make active a gold catalyst strongly depend on the preparation method [21].

Several reviews have been published over the past years and different results sometimes contradictory are reported [22,23]. Therefore, it is difficult to generalize and draw conclusions on the basis of data recorded from a wide variety of catalysts differently prepared and operating under different conditions.

The objective of the present work was to investigate the effect of the support on the activity in CO oxidation and in the preferential CO oxidation in the presence of hydrogen (PROX) of Au catalysts. To this aim, catalysts with 1.5 wt% gold loading were prepared over different types of reducible oxides (TiO_2, Co_3O_4–CeO_2, CeO_2 and Co_3O_4) and over a typical non-reducible support, like Al_2O_3. In order to investigate the effect of the support on structural, electronic and catalytic properties of the gold catalysts, the same preparation method, deposition precipitation by using Na_2CO_3 solution, was used. The pH of the suspension was optimized for the different supports, as a function of the point of zero charge (PZC). Characterizations by specific surface area measurements (BET), powder X-ray diffraction (XRD), transmission electron microscopy (TEM) and X-ray photoelectron spectroscopy (XPS) analyses were carried out. Catalytic tests in the CO oxidation and preferential CO oxidation in the presence of hydrogen (PROX) were performed.

* Corresponding author. Tel.: +39 091 6809371; fax: +39 091 6809399.
E-mail address: liotta@pa.ismn.cnr.it (L.F. Liotta).

0920-5861/$ – see front matter © 2010 Elsevier B.V. All rights reserved.
doi:10.1016/j.cattod.2010.04.049

2. Experimental

2.1. Catalyst preparation

Commercial oxides, TiO_2 (Eurotitania) and γ-Al_2O_3 (Aldrich) were used as supports.

Co-precipitation method was used to synthesize Co_3O_4, CeO_2 and Co_3O_4–CeO_2 mixed oxide with Co/Ce atomic ratio equal to 1, according to a published procedure [24]. Nitrate hexahydrate salts of cobalt and cerium (Aldrich, ≥98%) were dissolved in water solution under stirring. Aqueous Na_2CO_3 0.5 M was then slowly added until pH 8.5. The precipitate obtained was aged at room temperature for 3 h, followed by filtration and repeated washing with hot water. After drying at 120 °C overnight, the resulting powders were calcined at 600 °C for 4 h.

Au catalysts were prepared over the above supports by deposition–precipitation method. In a typical preparation, an appropriate amount of support was dispersed in a proper volume of 10^{-4} M $HAuCl_4$ solution, in order to obtain a gold loading of 1.5 wt%. The pH of the suspension was, then, adjusted with 0.05 M Na_2CO_3 solution to 7–8, depending on the PZC of the support, in order to optimize gold deposition and stabilization. After stirring for 2 h at room temperature, the powder was recovered by filtration and washed several times with hot water until no chloride ions were detected, as tested by 0.1 M $AgNO_3$ solution. The so obtained samples were dried at 120 °C overnight and, then, stored away from light and under vacuum in a desiccator, in order to prevent any alteration (as-prepared catalysts).

2.2. Catalyst characterization

Elemental analysis of the catalysts was performed by inductively coupled plasma optical emission spectroscopy (ICP-OES), using a ICP Perkin-Elmer Optima 3000DV spectrometer. The catalyst powder was dissolved in aqua regia + HF in a microwave oven.

A gold loading between 1.1 and 1.4 wt% was obtained, depending on the support (see Table 1).

The specific surface areas were determined by BET method from nitrogen adsorption isotherms at −196 °C using Sorptomatic 1900 (Carlo Erba) instrument.

The point of zero charge (PZC) of the supports was determined by powder titration method [25]. In the course of powder titration, subsequent portions of the oxide supports were added to an aqueous solution and the pH of the equilibrated dispersion was measured. The pH of the system changed gradually until a constant value of pH, which is equal to the point of zero charge.

Powder X-ray diffraction patterns were recorded at room temperature using a Bruker D5000 diffractometer with a copper target tube and a diffracted beam graphite monochromator selective for Cu Kα radiation (λ = 1.5418 Å). The assignment of the various crystalline phases was based on the JPDS powder diffraction file cards [26]. Mean crystallite size (d) of different phases was calculated from the line broadening of the most intense reflections using the Scherrer equation [27].

Transmission electron microscopy (TEM) analyses were performed on the powder catalysts by using a JEOL, JEM 2100 instrument working at 200 kV equipped with energy-dispersive spectrometer (EDS) for electron probe microanalysis. Suspensions of the samples in ethanol were dropped on carbon-coated grid and after evaporating the solvent electron micrographs of the particles were taken. The particle size distribution was obtained by measuring the diameter of about 200 particles.

The X-ray photoelectron spectroscopy analyses were performed with a VG Microtech ESCA 3000 Multilab, equipped with a dual Mg/Al anode. The spectra were excited by the unmonochromatised Al Kα source (1486.6 eV) run at 14 kV and 15 mA. The analyzer operated in the constant analyzer energy (CAE) mode. For the individual peak energy regions, a pass energy of 20 eV set across the hemispheres was used. Survey spectra were measured at 50 eV pass energy. The sample powders were analyzed as pellets, mounted on a double-sided adhesive tape. The pressure in the analysis chamber was in the range of 10^{-8} Torr during data collection. The constant charging of the samples was removed by referencing all the energies to the C 1s set at 285.1 eV, arising from the adventitious carbon. The invariance of the peak shapes and widths at the beginning and at the end of the analyses ensured absence of differential charging.

Analyses of the peaks were performed with the software provided by VG, based on non-linear least squares fitting program using a weighted sum of Lorentzian and Gaussian component curves after background subtraction according to Shirley [28] and Sherwood [29]. Atomic concentrations were calculated from peak intensity using the sensitivity factors provided with the software. The binding energy (BE) values are quoted with a precision of ±0.15 eV and the atomic percentage with a precision of ±10%.

2.3. Catalytic measurements

Catalytic tests in CO oxidation and in PROX were carried out using a quartz glass U-shaped reactor, equipped with a temperature programmed controller. Based on previous studies [16,30], before the CO oxidation tests the samples (50 mg) were pretreated "in situ" under flowing 5% O_2 in He (50 ml/min) at 120 °C for 30 min, while before PROX reactions, a reductive pretreatment under 5% H_2 in Ar at 150 °C during 30 min was performed.

The reactant mixture consisting of 1% CO + 1% O_2 in He or 70% H_2 + 1% CO + 1% O_2 in He, for CO oxidation or PROX, respectively, was led over the catalyst at a flow rate of 50 ml/min, equivalent to a weight hourly space velocity (WHSV) of 60,000 ml g^{-1} h^{-1}. The CO conversion and the selectivity in PROX reaction were calculated using an ABB infrared analyzer detector for CO and CO_2 and an ABB paramagnetic Magnos 206 for O_2. The CO converted was calculated on the basis of the CO_2 produced, whereas the selectivity was calculated according to the following equation [(CO conversion/2)/O_2 conversion × 100].

3. Results

3.1. Catalyst characterization

The X-ray diffraction spectra, in the angular range 20–70° 2θ, of as-prepared gold catalysts are shown in Fig. 1a. In Table 1 the textural properties are listed. Crystalline features of CeO_2 fluorite-type cubic structure along with peaks of Co_3O_4 spinel phase were detected. The TiO_2 was for the most part constituted of anatase, moreover a small peak typical of brookite (at $2\theta = 30.8°$) corresponding to the (1 2 1) diffraction plane was observed. The alumina exhibited rather broad peaks assigned to γ-phase. No (1 1 1) diffraction lines corresponding to the f.c.c. structure of gold were observed (see Fig. 1b), suggesting the presence of highly dispersed particles. However, we cannot exclude that the Au (1 1 1) reflection at 38.18° is undetectable due to the relatively low loading and because partially superimposed by the broad reflections of the supports (TiO_2, Co_3O_4). As it concerns the oxides crystallinity, nanoparticles ranging in size from 7 to 15 nm were obtained in all cases, as calculated from the line broadening of the most intense XRD peaks.

As listed in Table 1, the commercial supports, Al_2O_3 and TiO_2 exhibit high specific surface area (≥130 m^2/g), while for precipitated oxides, CeO_2, Co_3O_4–CeO_2 and Co_3O_4, area values around 40–50 m^2/g were measured. Moreover, the nature of the support oxide strongly influences the surface polarizability as indicated by the PZC values, which range between 5.8 and 8.0. Oxide surfaces

Table 1
Specific surface area (BET), PZC values, XRD and TEM derived particles size (d) of as-prepared gold catalysts.

Catalyst	Au (wt%)	BET (m^2/g)	PZC[a]	d_{oxide} (XRD) (nm)	d_{Au} (TEM) (nm)
Au/TiO_2	1.4	127	5.8	9.0	2.5 ± 1.0
$Au/Co_3O_4–CeO_2$	1.4	48	6.9	11.0 (Co_3O_4)9.0 (CeO_2)	2.9 ± 1.0
Au/CeO_2	1.4	52	6.5	7.0	2.9 ± 1.2
Au/Co_3O_4	1.3	39	7.2	15.0	–
Au/Al_2O_3	1.1	160	8.0	–	3.5 ± 2.1

[a] The point of zero charge (PZC) was measured on the supports.

usually exhibit both Brønsted and Lewis acidity and when dispersed in water solution become positively or negatively charged, depending on the pH. Thus, the PZC, corresponding to the condition where no net charge is present on the surface, is an important factor that controls the deposition of gold species. Accordingly, a dependence of the amount of gold deposited with the pH of the solution has been reported for different types of supports [21,23]. Our results also indicate the nature of the support and the pH of the solution (7–8) has an influence on the amount of deposited gold. In all cases, the gold loading was close to the nominal one, with the highest content (1.4 wt%) for TiO_2, $Co_3O_4–CeO_2$, CeO_2, while the yield of deposited gold slightly decreased for Co_3O_4, the lowest loading being for Au/Al_2O_3. There is general agreement that the maximum of gold loading is obtained when the pH is close to the PZC of the support [21]. The presence at pH > 6 of strongly adsorbing gold hydroxyl–chloride complexes has been suggested to explain the mechanism of gold deposition over TiO_2, γ-Al_2O_3 and goethite FeO(OH) [31–33]. Under the conditions of gold concentration (10^{-4} M) and at the pH used in our case, it is likely that a similar adsorption mechanism of anionic gold-complex species occurs, leading to high gold deposition yield. Moreover, the high surface area of our TiO_2 and/or the presence of structural defects in the small crystallites of $Co_3O_4–CeO_2$, CeO_2 and Co_3O_4 oxides could contribute to a higher interaction of the support with gold complexes. The lowest gold loading of 1.1 wt%, observed for Au/Al_2O_3 prepared at pH 8 close to the PZC, is not surprising looking at the literature. Different studies on Au/γ-Al_2O_3 catalysts prepared by DP with Na_2CO_3 solution, showed that the gold loading decreased at pH ≥ 8, probably because of the decreasing of hydroxyl groups [34,35].

Fig. 2a–d shows representative transmission electron micrographs of the catalysts Au/TiO_2 (a), $Au/Co_3O_4–CeO_2$ (b), Au/CeO_2 (c), Au/Al_2O_3 (d). The EDS analysis allowed the identification of the different phases in the samples. In Table 1 the gold particles size distribution derived by TEM analyses is reported. For Au/TiO_2 well-dispersed Au nanoparticles (black dots) with size 2.5 ± 1.0 nm can be seen along with TiO_2 patches with size between 6 and 8 nm (dark gray spots). $Au/Co_3O_4–CeO_2$ and Au/CeO_2 contain also small Au particles (d_{Au} around 2.9 ± 1.0 nm) and crystallites of Co_3O_4 and CeO_2 with mean diameter ~10 nm, which are located mostly in the vicinity of gold nanoparticles. Some isolated bigger clusters (~20 nm) of ceria, not in contact with gold, were also detected in the Au/CeO_2 catalyst. The Au particle size increased up to 5 nm over alumina, where a wider distribution ($d_{Au} = 3.5 \pm 2.1$) was observed.

The XPS results are summarized in Table 2 in terms of the Au $4f_{7/2}$ BE and of the support element main peak energies. The atomic percentage of each species is also given. The experimental Au 4f photoelectron spectra of the catalysts along with the corresponding curve fitting are shown in Fig. 3. In the case of $Au/Co_3O_4–CeO_2$ and Au/CeO_2 the curve fitting produced two components at BE = 85.0 ± 0.1 and 86.7 eV, which can be assigned to Au^+ and Au^{3+} species, respectively [16,36]. As indicated by the relative distribution of gold species (Table 2), cationic gold was predominantly present as Au^{3+} species (~80%). The XP spectra of Au/TiO_2 and Au/Al_2O_3 catalysts contain a main Au $4f_{7/2}$ component at 84.4 eV typical of metallic gold, which represents ~70% of the gold species present, the other one at 86.6 ± 0.1 eV attributed of Au^{3+} accounts for the remaining ~30%. In the case of Au/Co_3O_4 the curve fitting yielded one component only, characterised by Au$4f_{7/2}$ at 85.1 eV typical of ionic gold Au^+ [36].

The surface atomic ratios between gold and the support elements are also listed in Table 2 along with the analytical values, given in parentheses. All catalysts show a gold enrichment at the surface, particularly in the case of Au/TiO_2 and $Au/Co_3O_4–CeO_2$, suggesting high number of surface catalytic sites.

For each catalyst, the support element main peak binding energy, Ti$2p_{3/2}$, Ce$3d_{5/2}$ and Al2p is typical of the corresponding pure oxides, TiO_2, CeO_2, Al_2O_3 [37]. For CeO_2 and $Co_3O_4–CeO_2$ supported catalysts, the relative percentage of the two cerium species was estimated by the intensity of the Ce $3d_{5/2}$ components relative to Ce^{4+} (V, V′, V‴) and to Ce^{3+} (V′ and U′) [16,38]. It is worth noticing an increase of Ce^{3+} amount in the $Co_3O_4–CeO_2$ supported gold, which is indicative of a defective structure with high oxygen vacancies.

As it concerns the photoelectron spectra of the Co2p region contain two components characterized by binding energy at about 781.0 and 779.1 eV, typical of Co^{2+} and Co^{3+} species, respectively [24].

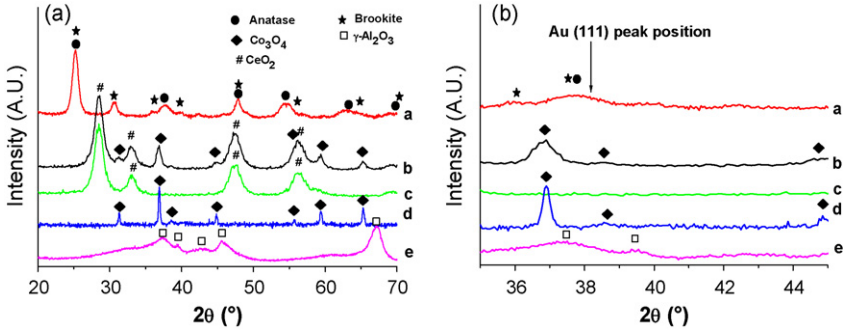

Fig. 1. Panel a, XRD patterns, in the angular range 20–70° 2θ, of Au supported catalysts: (a) Au/TiO_2, (b) $Au–Co_3O_4–CeO_2$, (c) Au/CeO_2, (d) Au/Co_3O_4, (e) Au/Al_2O_3. Panel b, enlargement in the angular range 35–45° 2θ.

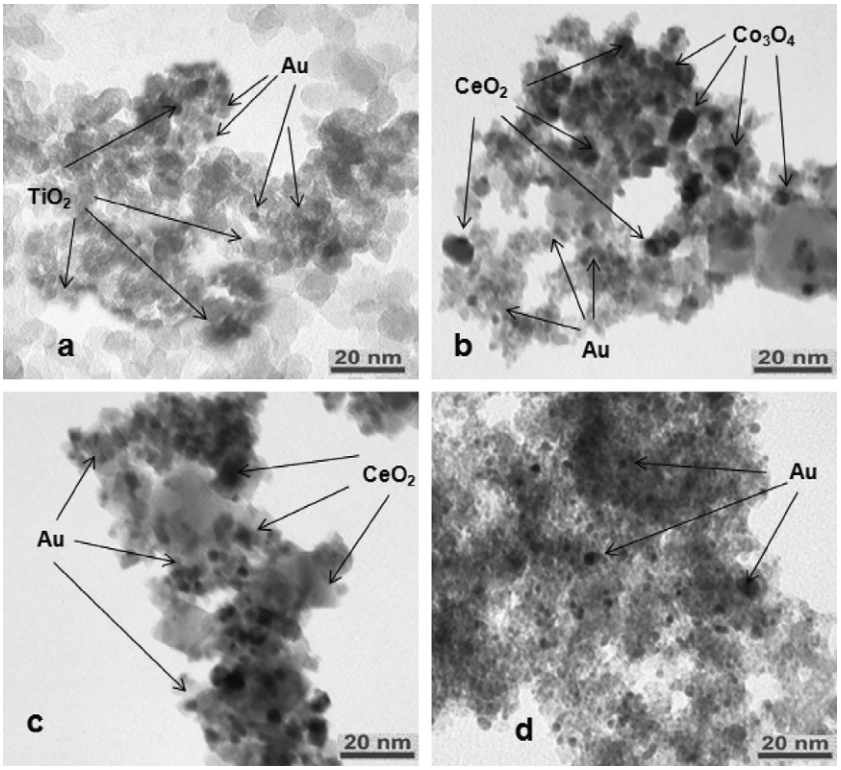

Fig. 2. Typical TEM micrographs of supported gold catalysts: (a) Au/TiO_2; (b) $Au/Co_3O_4–CeO_2$; (c) Au/CeO_2; (d) Au/Al_2O_3.

Table 2
XPS binding energies of gold and main support peaks and atomic ratio of gold over support elements. The atomic percentage of each species is given in parenthesis.

Samples	Au $4f_{7/2}$ (eV)	Ti $2p_{3/2}$ (eV)	Ce $3d_{5/2}$ (eV)	Co $2p_{3/2}$ (eV)	Al 2p	Au/Me[a]
Au/TiO_2	84.4 (75%); 86.5 (25%)	459.0	–	–	–	0.03 (0.006)
$Au/Co_3O_4–CeO_2$	85.1 (80%); 86.7 (20%)	–	882.4 (87%); 885.5 (13%)	779.2 (45%); 780.8 (55%)	–	[0.18 (0.013) M = Co]; [0.06 (0.017) M = Ce]
Au/CeO_2	84.9 (77%); 86.7 (23%)	–	881.3 (95%); 883.7 (5%)	–	–	0.016 (0.012)
Au/Co_3O_4	85.1 (100%)	–	–	779.1 (50%); 780.8 (50%)	–	0.02 (0.005)
Au/Al_2O_3	84.4 (69%); 86.7 (31%)	–	–		75.0	0.005 (0.003)

[a]Me = Ti, Co, Ce, Al; in parenthesis the analytical ratios (determined by ICP-OES) are given.

3.2. Catalytic activity and selectivity

The catalytic performances of gold supported catalysts in the CO oxidation are shown in Fig. 4. In Table 3, the temperature in correspondence of 50% CO conversion (T_{50}) are listed. Au/TiO_2 was the most active catalyst giving nearly 90% of CO conversion at 25 °C, followed by $Au/Co_3O_4–CeO_2$ achieving almost full conversion at 75 °C. Au/CeO_2 and Au/Co_3O_4 were slightly less performing, while for Au/Al_2O_3 the 100% value of conversion was achieved at 250 °C. According to our previous results [39] $Co_3O_4–CeO_2$ and Co_3O_4 showed appreciable CO conversion at $T > 150$ °C and CeO_2 above 300 °C, therefore the activity of the supports only is not discussed in the paper.

In Fig. 5a and b the degree of CO conversion and the selectivity toward CO_2 in the PROX reaction are compared for gold supported catalysts. In Table 4 the selectivity towards CO_2, achieved at the maximum CO conversion value, are listed. By comparing Figs. 4 and 5a, it results that $Au/Co_3O_4–CeO_2$ and Au/CeO_2 showed the same high CO oxidation activity in presence of H_2 and without, attaining 50% of CO conversion at the same temperature as reported in Table 3. Moreover, both catalysts gave at 100 °C around 80% of CO conversion with a selectivity of 49% and 40%, respectively (Table 4). Surprisingly, Au/TiO_2 does not perform as well as in CO oxidation. At 50 °C a maximum CO conversion of 53% was achieved and selectivity of 46%, but increasing the temperature the CO oxidation was weakened by the competition with H_2 oxidation, according to a drastic decrease of selectivity. In the case of Au/Co_3O_4, at low temperature, up to ~80 °C, the CO conversion runs similarly with and without H_2 (Figs. 4 and 5a), while at higher tem-

Table 3
Temperature (°C) in correspondence of 50% CO conversion in the CO oxidation. Reaction mixture 1% CO +1% O_2 in He, WHSV of 60,000 ml g^{-1} h^{-1}.

Catalyst	T_{50} (°C)
Au/TiO_2	<25
$Au/Co_3O_4–CeO_2$	36
Au/CeO_2	59
Au/Co_3O_4	84
Au/Al_2O_3	125

Table 4
Maximum CO conversion and corresponding selectivity values towards CO_2 in PROX reaction in the range of temperature 50–100 °C.

Catalyst	Temperature (°C)	Maximum CO conversion (%)	Selectivity (%)
Au/TiO_2	50	53	46
$Au/Co_3O_4–CeO_2$	100	80	49
Au/CeO_2	100	76	40
Au/Co_3O_4	100	43	21
Au/Al_2O_3	80	42	25

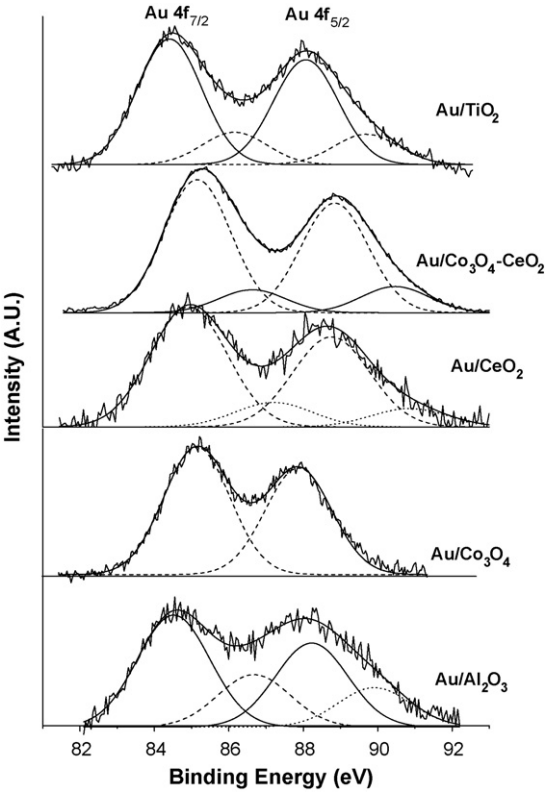

Fig. 3. Experimental and fitted Au 4f photoelectron spectra of Au supported catalysts.

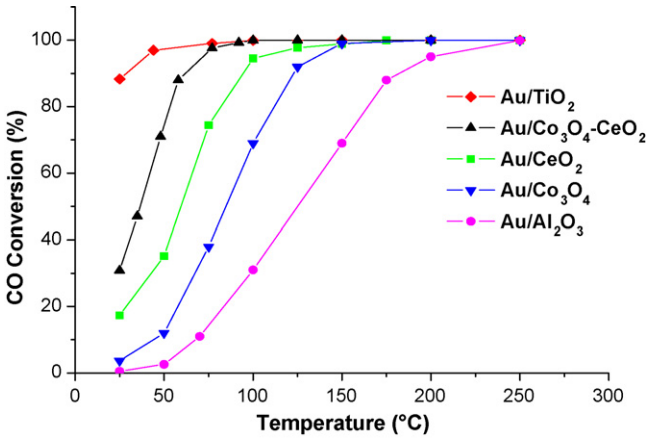

Fig. 4. CO conversion (%) as a function of temperature for Au supported catalysts. Reaction mixture: 1% CO + 1% O_2, He as balance.

perature the CO consumption diminished with parallel dropping of the selectivity.

Au/Al_2O_3 was an exception showing in presence of hydrogen an increased CO oxidation activity at low temperature, converting 42% of CO at 80 °C with a selectivity of 25%. By increasing the temperature, activity and selectivity towards CO oxidation drastically decreased (Fig. 5; Table 4).

4. Discussion

Although, the nature of active sites for the activity of gold based catalysts in CO oxidation and PROX reaction has been a matter of controversial discussion in the last years [23], there is a general agreement about the main factors responsible for the activity. Among all of them, the nature of gold species and particles size, the metal oxide support, reducible or non-reducible, and the perimeter interface between gold and the support play a fundamental role [15,17,40–43]. Based on these findings, an explanation of the different catalytic behavior of gold supported catalysts in CO oxidation and PROX is proposed. Au/TiO_2, the better performing catalyst in CO oxidation, contains highly dispersed gold sites at the catalyst surface along both species Au^0 and Au^{3+}, which were claimed important for achieving high CO oxidation activity [15,17]. Concerning the oxygen activation, a Langmuir–Hinshelwood mechanism has been proposed where oxygen dissociation at the interface between gold particle-support occurs [44]. As a result, the length of perimeter interface Au-reducible oxide was regarded as fundamental [20]. On these bases, the high dispersion of gold nanoparticles achieved over nanosized titania, leading to a high population of low coordinated atoms, is consistent with the good oxidation activity. Moreover, it is likely that in Au/TiO_2 catalyst the small particle size of titania (d_{TiO_2} = 9 nm, Table 1) contributes to increase the interface gold/active sites [20].

In the case of Au/CeO_2, in addition to the perimeter effect, the activity in CO oxidation was ascribed to the nature of the support. Ceria is well known for its oxygen storage capacity and the role of surface vacancies in activating superoxide molecular species has been clearly demonstrated in the CO oxidation reaction over supported gold catalysts [45,46]. Moreover due to the easy reducibility typical of small crystallites (d_{CeO_2} = 7 nm, Table 1), ceria can also

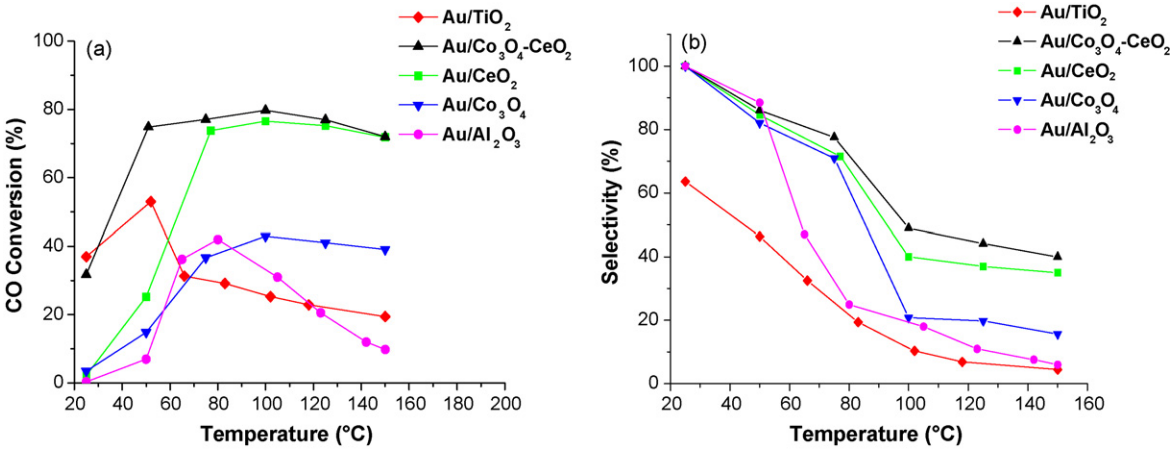

Fig. 5. Comparison between the CO conversion (a) and the selectivity towards CO_2 (b) over Au supported catalysts. Reaction mixture: 70% H_2 + 1% CO + 1% O_2, He as balance.

act as an oxygen supplier with a Mars–van Krevelen mechanism [47]. The presence of ionic Au^{3+}/Au^{+} species strongly interacting with ceria would increase the CO oxidation activity [16,36].

The superior catalytic performance of $Au/Co_3O_4–CeO_2$ with respect to Au/CeO_2 is consistent with an increase of oxygen vacancies in the mixed oxide and a higher dispersion of gold sites at the surface (Table 2).

Deposition of gold over Co_3O_4 resulted in Au^{+} species only. The electronic state of gold, less oxidized than in $Au/Co_3O_4–CeO_2$ and Au/CeO_2 catalysts, associated with the lower reducibility of un-promoted Co_3O_4 with respect to the $Co_3O_4–CeO_2$ system [24] may account for a less performing catalyst. As it concerns the relatively low CO oxidation activity of Au/Al_2O_3, as compared to gold over reducible oxides, this result is in agreement with the lowest amount of gold detected for this sample and in line with the literature [23,48].

Moving to activity and selectivity of gold supported catalysts in the PROX, it is worth noting that the presence of excess hydrogen leads to conditions different from those in the CO oxidation, with oxygen vacancies formation in reducible oxides. At the relatively low temperature of the PROX reaction, it has been demonstrated that surface oxygen vacancies play a major role in promoting CO oxidation and their generation was enhanced by the lower temperature region reducibility of gold catalysts supported on ceria modified by rare earths [30]. Accordingly, $Au/Co_3O_4–CeO_2$ and Au/CeO_2 exhibited at 100 °C the best results both, on activity and selectivity (Table 4). Moreover, both catalysts showed almost stable CO conversion of 72% up to 150 °C and selectivity around 35–40%. Au/Co_3O_4 performs similarly as in the CO oxidation, giving appreciable CO conversion only above ~75 °C, where H_2 oxidation occurs in competition with consequent low selectivity towards CO_2.

In the case of Au/TiO_2, the best performing in the CO oxidation, the presence of excess oxygen leads to a significant change in the CO conversion, which seems significantly affected by the competition with H_2. It is likely that the large population of highly dispersed and low coordinate surface Au atoms activate oxygen, which at low-temperature reacts with both, CO and H_2, by increasing the temperature the hydrogen oxidation becomes predominant [49,50].

The increased CO oxidation activity at low-temperature observed for Au/Al_2O_3 in the PROX reaction is consistent with the literature [48,51] and it is likely that formation of highly oxidizing intermediates at the perimeter of the Au nanoparticles with the support can occur.

5. Conclusions

Au catalysts supported on reducible oxides (TiO_2, $Co_3O_4–CeO_2$ CeO_2 and Co_3O_4) were studied in the CO oxidation and PROX reaction and compared with Au over a non-reducible oxide, Al_2O_3. The properties of the resulting catalysts, in terms of gold loading, electronic state of gold species and catalytic performances depend on the nature of the support.

As shown by TEM investigations Au particle sizes around 2.5–3 nm were obtained over reducible oxides, while Au/Al_2O_3 contains bigger gold particles (up to 5 nm) confirming the idea that gold over a non-reducible oxide gives a weak metal-support interaction.

$Co_3O_4–CeO_2$ and CeO_2 reducible oxides stabilize Au^{3+}/Au^{+} ionic species and produced active gold catalysts for CO oxidation and the best performing systems in PROX reaction. The presence of oxygen vacancies and/or their generation in excess of hydrogen plays a major role in the high activity and good selectivity of such catalysts.

The superior CO oxidation activity of Au/TiO_2 was ascribed to the presence of both species, nanosized metallic gold particles and Au^{3+} ions, which interacting with titania provide active sites for CO and oxygen dissociation. However, in presence of excess of hydrogen, CO oxidation was almost suppressed by the strong competition between H_2 and CO for adsorption and reaction with the activated oxygen atoms. As compared to $AuCo_3O_4–CeO_2$ and Au/CeO_2, Au/Co_3O_4 was less performing in CO oxidation and PROX as well.

The presence of gold particles over Al_2O_3, a non-reducible support, has proven to give poor catalytic activity.

Acknowledgements

Support by European Community, through the Network of Excellence (NoE) IDECAT (integrated Design of Catalytic Nanomaterials for a Sustainable Production) and COST D36 action is acknowledged.

References

[1] F. Marschner, F.W. Moeller, in: B.E. Leach (Ed.), Applied Industrial Catalysis, vol. 2, Academic Press, New York, 1983.
[2] D.L. Trimm, Appl. Catal. A 296 (2005) 1.
[3] H.P. Dhar, L.G. Christner, A.K. Kush, J. Electrochem. Soc. 134 (1987) 3021.
[4] S.H. Lee, J. Han, K.-Y. Lee, J. Power Sources 109 (2002) 394.
[5] J.L. Ayastuy, A. Gel-Rodriguez, M.P. Gonzales-Marcos, M.A. Guitierres-Ortz, Int. J. Hydrogen Energy 31 (2006) 2231.
[6] M. Sonza, N. Ribeiro, M. Schmal, Int. J. Hydrogen Energy 32 (2007) 425.
[7] D. Cameron, R. Holliday, D. Thompson, J. Power Sources 118 (2003) 298.
[8] M.M. Schubert, A. Venugopal, M.J. Kahlich, V. Plzak, R.J. Behm, J. Catal. 222 (2004) 32.
[9] B. Schumacher, Y. Denkwitz, V. Plzak, M. Kinne, R.J. Behm, J. Catal. 224 (2004) 449.
[10] L.-H. Cheng, Y.-L. Yeh, Y.-W. Chen, Int. J. Hydrogen Energy 33 (2008) 1965.
[11] R.J.H. Grisel, B.E. Nieuwenhuys, J. Catal. 199 (2001) 48.
[12] R.J.H. Grisel, C.J. Weststrate, A. Goossens, M.W.J. Craje, A.M. Van der Kraan, B.E. Nieuwenhuys, Catal. Today 72 (2002) 123.
[13] B. Schumacher, V. Plzak, K. Kinne, R.J. Behm, Catal. Lett. 2003 (2003) 109.
[14] G.R. Bamwenda, S. Tsubota, T. Nakamura, M. Haruta, Catal. Lett. 44 (1997) 83.
[15] G.C. Bond, D.T. Thompson, Gold Bull. 33 (2000) 41.
[16] A.M. Venezia, G. Pantaleo, A. Longo, G. Di Carlo, M.P. Casaletto, F.L. Liotta, G. Deganello, J. Phys. Chem. B 109 (2005) 2821.
[17] L. Delannoy, N. Weiher, N. Tsapatsaris, A.M. Beesley, L. Nchari, Sven L.M. Schroeder, C. Louis, Top. Catal. 44 (2007) 263.
[18] M. Haruta, S. Tsubota, T. Kobayashi, H. Kageyama, M.J. Genet, B. Delmon, J. Catal. 144 (1993) 175.
[19] S. Arii, F. Mortin, A.J. Renouprez, J.L. Rousset, J. Am. Chem. Soc. 126 (2004) 1199.
[20] A. Beck, A. Horváth, Gy. Stefler, R. Katona, O. Geszti, Gy. Tolnai, L.F. Liotta, L. Guczi, Catal. Today 139 (2008) 180.
[21] A. Wolf, F. Schüth, Appl. Catal. A 226 (2002) 1.
[22] M.S. Chen, D.W. Goodman, Acc. Chem. Res. 39 (2006) 739.
[23] G.C. Bond, C. Louis, D. Thompson, Catalysis by Gold, Catalytic Science Series, vol. 6, Imperial College Press, London, 2006.
[24] L.F. Liotta, G. Di Carlo, G. Pantaleo, A.M. Venezia, G. Deganello, Appl. Catal. B 66 (2006) 217.
[25] V. La Parola, G. Deganello, S. Scirè, A.M. Venezia, J. Solid State Chem. 174 (2003) 482.
[26] JCPDS Powder Diffraction File. PDF-2 Database. Int. Centre for Diffraction Data, Swarthmore, USA, 2000.
[27] H.P. Klug, L.E. Alexander, X-ray Diffraction Procedures for Polycrystalline and Amorphous Materials, Wiley, New York, 1954.
[28] D.A. Shirley, Phys. Rev. B 5 (1972) 4709.
[29] P.M.A. Sherwood, in: D. Briggs, M.P. Seah (Eds.), Practical Surface Analysis, Wiley, New York, 1990, p. 181.
[30] L. Ilieva, G. Pantaleo, I. Ivanov, R. Zanella, A.M. Venezia, D. Andreeva, Int. J. Hydrogen Energy 34 (2009) 6505.
[31] F. Moreau, G.C. Bond, A.O. Taylor, J. Catal. 231 (2005) 105.
[32] M.L. Machesky, W.O. Andrade, A.W. Rose, Geochim. Cosmochim. Acta 5 (1991) 769.
[33] C. Cellier, S. Lambert, E.M. Gaigneaux, C. Poleunis, V. Ruaux, P. Eloy, C. Lahousse, P. Bertrand, J.-P. Pirard, P. Grange, Appl. Catal. B 70 (2007) 406.
[34] S.-J. Lee, A. Gavriilidis, J. Catal. 206 (2002) 305.
[35] R.J.H. Grisel, P.J. Kooyman, B.E. Nieuwenhuys, J. Catal. 191 (2000) 430.
[36] M.P. Casaletto, A. Longo, A. Martorana, A. Prestianni, A.M. Venezia, Surf. Interface Anal. 38 (2006) 215.
[37] J.F. Moulder, W.F. Stickle, P.E. Sobol, K.D. Bomben, in: J. Chastain, R.C. King Jr. (Eds.), Handbook of X-ray Photoelectron Spectroscopy, Phys. Electronics Inc., Eden Prairie, USA, 1995.
[38] A. Kotani, T. Jo, J.C. Parlebas, Adv. Phys. 37 (1988) 37.
[39] L.F. Liotta, G. Di Carlo, A. Longo, G. Pantaleo, A.M. Venezia, Catal. Today 139 (2008) 174.
[40] M. Haruta, Catal. Today 36 (1997) 153.
[41] G. Bond, D. Thompson, Catal. Rev. Sci. Eng. 41 (1999) 319.
[42] M. Haruta, M. Daté, Appl. Catal. A 222 (2001) 427.

[43] T.V. Choudhary, D.W. Goodman, Top. Catal. 21 (2002) 25.
[44] L.M. Molina, M.D. Rasmussen, B. Hammer, J. Chem. Phys. 120 (2004) 7673.
[45] M. Okumura, Y. Kitagawa, M. Haruta, K. Yamaguchi, Appl. Catal. A 291 (2005) 37.
[46] D. Widmann, R. Leppelt, R.J. Behm, J. Catal. 251 (2007) 437.
[47] A.C. Gluhoi, H.S. Vreeburg, J.W. Bakker, B.E. Nieuwenhuys, Appl. Catal. A 291 (2005) 145.
[48] E. Quinet, F. Morfin, F. Diehl, P. Avenir, V. Caps, J.-L. Rousset, Appl. Catal. B 80 (2008) 195.
[49] H. Imai, M. Daté, S. Tsubota, Catal. Lett. 124 (2008) 68.
[50] A. Beck, A. Horváth, G. Stefler, M.S. Scurrell, L. Guczi, Top. Catal. 52 (2009) 912.
[51] D. Gavril, A. Georgaka, V. Loukopoulos, G. Karaiskakis, B.E. Nieuwenhuys, Gold Bull. 39 (2006) 192.